Baghdad Science Journal

Volume 23 | Issue 5 Article 23

5-29-2026

Investigating the Effect of Functional Group on Folic Acid Conjugation and *in vitro* Characteristics of Lomustine from Silica Nanoparticles

Areen M. Khattabi
Pharmacological and Diagnostic Research Center (PDRC), Faculty of Pharmacy, Al-Ahliyya Amman University, Amman, Jordan, 19111, a.khattabi@ammanu.edu.jo

Lina M. Ibraheem
Department of Pharmaceutical Sciences and Pharmaceutics, Faculty of Pharmacy, Applied Science Private University, Amman, Jordan, Post Code: 11937, barre.lina187@gmail.com

Eman M. Migdadi
Department of Pharmaceutical Sciences and Pharmaceutics, Faculty of Pharmacy, Applied Science Private University, Amman, Jordan, Post Code: 11937, e_migdadi@asu.edu.jo

How to Cite this Article

Khattabi, Areen M.; Ibraheem, Lina M.; and Migdadi, Eman M. (2026) "Investigating the Effect of Functional Group on Folic Acid Conjugation and *in vitro* Characteristics of Lomustine from Silica Nanoparticles," *Baghdad Science Journal*: Vol. 23: Iss. 5, Article 23.
DOI: https://doi.org/10.21123/2411-7986.5307

BAGHDAD SCIENCE JOURNAL 2026;23(5):1868–1880

Scan the QR to view the full-text article on the journal website

RESEARCH ARTICLE

Investigating the Effect of Functional Group on Folic Acid Conjugation and *in vitro* Characteristics of Lomustine from Silica Nanoparticles

Areen M. Khattabi [1,*], **Lina M. Ibraheem** [2], **Eman M. Migdadi** [2]

[1] Pharmacological and Diagnostic Research Center (PDRC), Faculty of Pharmacy, Al-Ahliyya Amman University, Amman, Jordan, 19111
[2] Department of Pharmaceutical Sciences and Pharmaceutics, Faculty of Pharmacy, Applied Science Private University, Amman, Jordan, Post Code: 11937

ABSTRACT

Herein, silica nanoparticles (SNs) with different functional groups (propyl amine, propyl thiol, propyl carboxylic acid and unmodified hydroxyl) were loaded with the anticancer agent lomustine (LMS) and conjugated with Folic Acid (FA) to produce FA-NH_2-SNs, FA-SH-SNs, FA-COOH-SNs, and FA-OH-SNs, respectively. The nanoparticles (NPs) were characterized using Fourier Transform Infrared Spectroscopy (FTIR) and Dynamic Light Scattering (DLS). Encapsulation Efficiency (EE) and drug release rate were measured using UV Spectrophotometer. The *in vitro* cytotoxicity toward HeLa and VERO cells was assessed using MTT assay. LMS encapsulation efficiency exceeded 40% and FTIR spectra confirmed a successful conjugation with FA. Particle size increased after LMS loading and FA conjugation, ranging from 284 to 308 nm. Zeta potential measurements showed that all NPs became more negative after FA conjugation. The largest shift occurred in NH_2-SNs, changing from about − 4 to −14 mV. One-way ANOVA showed statistically significant differences ($p < 0.05$) among most formulations for drug release rates and cytotoxicity which were lower compared to free drug. The cytotoxicity was higher against HeLa compared to VERO cells due to folate-receptor targeting. The order of cell toxicity effect was almost related to their release rate behaviors where FA-NH_2-SNs exhibited the lowest percentages (18% and 40%, respectively). Thus, the type of surface functional group significantly influenced the efficiency of FA conjugation, which in turn modulated the *in vitro* characteristics of the loaded drug where higher conjugation correlated with reduced release rates and cytotoxicity.

Keywords: Cumulative release, Cytotoxicity, DLS analysis, FTIR, Lomustine, Silica nanoparticles, Surface functionalization

Introduction

Nanotechnology is revolutionizing drug delivery by offering innovative solutions to some of the biggest therapeutic challenges. This field focuses on tiny particles known as nanoparticles (NPs). NPs are solid particles or particulate dispersions that range from 1–1000 nm, and drugs can be dissolved, entrapped, encapsulated, or attached to their matrix.[1] When designed as delivery systems, NPs achieve several goals. One main objective is to modify their surface properties to improve targeting and control drug release during transit and at the site of action.[2] This approach also reduces off-target toxicity, enhances therapeutic efficiency, and protects drugs from rapid degradation or clearance.[3] Different NPs have been developed for pharmaceutical applications. They are commonly classified by size, shape, and physicochemical characteristics.[4] Among these systems, silica nanoparticles (SNs) have attracted significant attention.[5,6] They are inorganic materials with highly ordered mesoporous structures resembling a honeycomb.[7] Recent studies show that SNs possess high surface area, large pore volume, dual internal/external functional surfaces,

Received 8 June 2025; revised 5 January 2026; accepted 19 January 2026.
Available online 29 May 2026

* Corresponding author.
E-mail addresses: a.khattabi@ammanu.edu.jo (A. M. Khattabi), barre.lina187@gmail.com (L. M. Ibraheem), e_migdadi@asu.edu.jo (E. M. Migdadi).

https://doi.org/10.21123/2411-7986.5307

and tunable morphology, making them superior drug carriers, particularly for cancer therapy.[7,8] Therapeutic agents can be loaded inside mesopores or attached to the outer surface, resulting in higher drug-loading capacity. Furthermore, the exterior silanol groups can be chemically functionalized with ligands to enhance targeting specificity.[9,10]

Targeted drug delivery increases the accumulation of therapeutic agents in specific cells, improving efficacy while limiting toxicity. This is mainly accomplished by conjugating the delivery system with ligands that bind selectively to receptors overexpressed at disease sites.[10,11] Several targeting ligands have been investigated, including folic acid (FA), peptides, aptamers, carbohydrates, and antibodies.[12] FA (vitamin B9) is of particular interest due to its biological importance, ease of conjugation, high receptor affinity, and excellent stability.[13] It plays a key role in cell proliferation and nucleotide synthesis and is transported via receptor-mediated endocytosis involving folate receptors (FRs).[14]

FRs are overexpressed in many cancers, including ovarian, breast, lung, brain, colon, and renal tumors, while showing limited expression in normal tissues, making FA an effective targeting ligand.[15] Its small size, chemical stability, and compatibility with diverse solvents further support its use in drug-delivery systems.[16] FA has been conjugated to many nanocarriers such as liposomes, polymers, dendrimers, carbon nanotubes, and SNs.[17]

In this study, FA was conjugated to four different surface-functionalized SNs: propyl amine (NH_2-SNs), propyl thiol (SH-SNs), propyl carboxylic acid (COOH-SNs), and unmodified silica (OH-SNs). The goal was to evaluate how the surface functional group influences FA conjugation and, consequently, the *in vitro* behavior of the loaded drug. Lomustine (LMS) was selected as the model drug, which has previously been loaded into superparamagnetic iron oxide NPs (SPIONs), PLGA NPs, and chitosan systems.[18,19] However, limited work has examined FA-conjugated SNs loaded with LMS, and no study has compared these four functional groups regarding FA conjugation efficiency, drug-release behavior, and cytotoxicity.

LMS (CCNU; 1-(2-chloroethyl)-3-cyclohexyl-1-nitrosourea) is an alkylating nitrosourea used to treat brain tumors, lung cancer, melanoma, lymphomas, and other solid tumors.[19] It induces apoptosis by sensitizing tumor cells and promoting TRC8-mediated degradation of heme oxygenase-1.[20] Despite its effectiveness, LMS suffers from dose-related toxicities. Its hydrophobicity also complicates intravenous administration, leading to severe side effects such as respiratory failure and vascular embolism. Therefore, developing safer and more effective delivery systems is essential to improve its therapeutic profile.

Materials and methods

Materials

Propyl amine silica NPs (particle size 200 nm, pore diameter 4 nm) were purchased from Nanoshell company UK. Unmodified silica NPs (particle size 200 nm, pore diameter 4 nm), propyl thiol silica NPs (particle size 200 nm, pore diameter 4 nm), propyl carboxylic acid silica NPs (particle size 200 nm, pore diameter 4 nm), phosphate buffer saline (BPS), FA, ethyl-3-(3-dimethylaminopropyl)carbodiimide (EDC), N-Hydroxysuccinimide (NHS) and DCC (dicyclohexyl carbodiimide) were obtained from Sigma Aldrich. LMS (purity $\geq$ 97%) was purchased from a genetics company. Cell culture components were obtained from Caisson Laboratories. Penicillin-Streptomycin and gentamicin sulfate were purchased from Euro-Clone Italy, while Trypsin – EDTA and fetal calf serum were provided by Biowest.

Methods

Preparation of LMS stock solution and LMS loaded SNs

LMS stock solution of 1 mg/mL concentration was first prepared in methanol. The stock solution was then diluted with methanol to get the standard solutions used for the calibration curve at the concentrations of 0.5, 1, 5, 10, 20, and 50 ug/mL.[20] For the loading process, a precise amount (0.01 g) of four different samples of SNs (NH_2-SNs), (SH-SNs), (COOH-SNs), and (OH-SNs), (shown in Fig. 1), were mixed separately with 4 mL of LMS stock solution (1 mg/mL) and stirred for 24 hours. The collected NPs were then centrifuged for about 25 minutes at 14000 rpm. The supernatant from each sample was used directly to measure encapsulation efficiency, while the resulting NPs were washed thoroughly with deionized water and dried.

Evaluation of the encapsulation efficiency of the SNs

The absorbance of the supernatants collected from each sample was eventually measured by a UV spectrophotometer at 230 nm (LMS $\bar{\lambda}$ max).[21] The EE of each sample was calculated using the following equation:

EE% = (weight of initially added drug – weight of free drug in supernatant)/weight of initially added

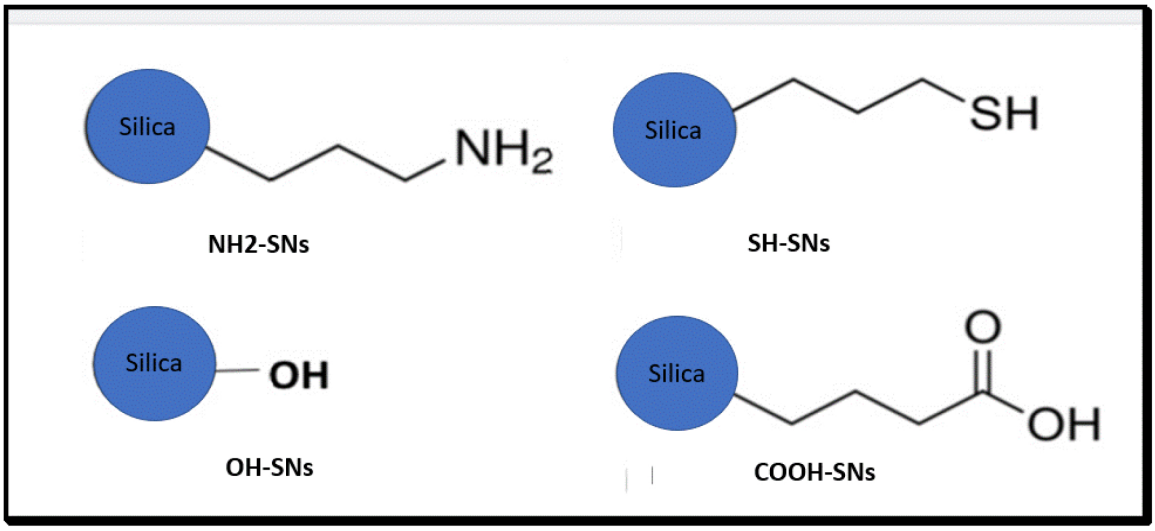

Fig. 1. Four different surface functionalizations of commercially available SNs were used: propyl amine (NH_2-SNs), propyl thiol (SH-SNs), propyl carboxylic acid (COOH-SNs), and unmodified hydroxyl (OH-SNs). All SNs have a particle size of approximately 200 nm and a pore diameter of about 4 nm.

drug × 100 %.[21] The measurements were performed in triplicate, and the mean was finally taken.

Modification of NH_2-SNs with FA

In 4 mL of ethanol, 0.005 g of NH_2-SN2 was mixed with 0.005 g of FA and 0.01 g of EDC and stirred for 24 hours at room temperature. The NPs were collected, rinsed with deionized water, centrifuged for 25 minutes at 14000 rpm, and dried overnight at T = 80 ˚C to obtain FA-NH_2-SNs.

Modification of SH-SNs with FA

A certain amount of SH-SNs (0.005 g) was mixed with 0.005 g of FA in 2 mL of dichloromethane for a few minutes, then 0.01 g of DCC was added with the other 2 mL of dichloromethane, and the reaction was allowed to stir for 24 hours at room temperature.[22] The resulting NPs were collected, washed with deionized water/acetone, and centrifuged at 14000 rpm for 25 minutes, then dried overnight at T = 80˚C to finally obtain FA-SH-SNs.

Modification of COOH-SNs with FA

A specific amount of COOH-SNs (0.005 g) was mixed in 4 mL of ethanol with 0.005 g of FA and 0.01 g of EDC and stirred for 24 hours at room temperature. The resulting NPs were collected, rinsed with deionized water, centrifuged for 25 minutes at 14000 rpm, and then dried overnight at T = 80 ˚C to obtain FA-COOH-SNs.

Modification of OH-SNs with FA

In PBS buffer solution (pH 6 and approximately 4 mL), 0.005 g of FA was activated with 0.005 g of EDC and 0.015 g NHS. The pH of the solution was raised to 8.5 by adding NaOH after stirring for 1–1.5 hours at room temperature. After that, a certain amount of SNs (0.005 g) was added and mixed overnight. The NPs were collected, rinsed with deionized water, centrifuged for 25 mins at 14000 rpm, and then dried overnight at T = ˚C to obtain FA-OH-SNs.[23]

FITR analysis

The FTIR spectra of free FA, unconjugated and FA conjugated SNs, suspended in the KBr matrix, were obtained in the mid-IR range (500–4000 cm^{-1}) using a WQF - 521 Fourier Transform Infrared spectrophotometer. However, the absorption bands caused by the functional groups of our added compounds appeared mainly in the range of 1000–3500 cm^{-1}.

DLS analysis

Diluted suspensions of SNs (5 × 10^{-4} mg/mL) were characterized using the DLS technique (Zetasizer Nano series, Malvern, U.K.) by measuring their mean particle size, PDI, and zeta potential. The samples were vortexed and analyzed before and after LMS loading and FA conjugation in PBS with a refractive index of 1.326 for PBS and 1.48 for SNs and viscosity = 1.2 Pa.s. The measurements were carried out in

triplicate with ten runs for each, and the mean was finally taken.

Assessment of in vitro drug release

A certain quantity of FA conjugated SNs loaded with LMS (0.005 g) were placed in a dialysis bag (Dialysis Tubing-MWCO-12-14000 Daltons) and mixed with 2 mL of PBS (pH = 7.4). Then they were transferred to a beaker containing 23 mL PBS and shaken inside a water bath at 37 °C. At various time intervals (1, 2, 3, 4, 6, 24, 25, 26, 28), a sample of 1 mL was drawn and replaced with fresh PBS. The amount of LMS released was measured using a UV spectrophotometer by measuring the absorbance at $\bar{\lambda}$ = 230 nm for LMS. The corresponding drug concentration was calculated based on the calibration curves obtained in PBS. The cumulative percentages of the released drug were then calculated for each sample, and the values represent the average of three experiments. The free drug was treated similarly.

Antiproliferative (cell viability) assay

Frozen HeLa as well as VERO cells were carefully thawed in a water bath at 37 °C, resuspended in cell culture media, and incubated for 24 hours. The cells were then detached with trypsin and counted under aseptic conditions. HeLa and VERO cells (100 μl/well), at an optimum concentration of 1000 cells/well, were dispersed separately into 96-well tissue culture flasks containing tissue culture medium including DMEM media for HeLa and MEM media for VERO, 10% fetal bovine serum, 1% penicillin-streptomycin, 1% L-glutamine and 0.1% gentamicin. The medium was withdrawn after 24 hours, and 200 μl of 0.15 mg/mL suspensions of LMS-loaded FA conjugated SNs, as well as free LMS, were added separately to the cells in triplicate and cultured for 48 hours. The MTT (3-(4,5-Dimethylthiazol-2-yl)-2,5-diphenyltetrazolium bromide) test was then used to evaluate the cell viability. From each well, 100 μl of culture media was removed, and 10 μl of thiazolyl blue tetrazolium solution was added to the wells and left in a CO_2 incubator for at least 3 hrs. Finally, to terminate the reaction, MTT solubilization solution (100 μl/well) was added, mixed thoroughly, and incubated for 1 more hour. To quantify the cell toxicity percentage, absorbance was measured at 550 nm using a microplate reader, and cell viability was determined to obtain the percentage of cell toxicity.

Statistical Analysis: All experiments were performed in triplicate, and data are presented as mean ± SD (n = 3). One-way ANOVA was used to compare the means of two or more samples and to determine the corresponding p-values to assess whether the differences were statistically significant.

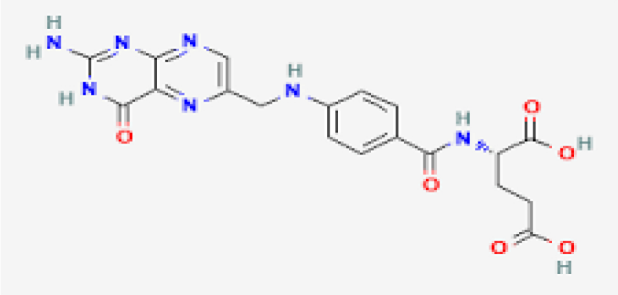

Fig. 2. Folic acid structure (https://pubchem.ncbi.nlm.nih.gov/).

Results and discussion

Measuring the encapsulation efficiency of SNs

Encapsulation efficiency refers to the actual content of material (drug) loaded into the NPs. As mentioned in the experimental part, the concentration of LMS was directly measured using UV spectroscopy at 230 nm by applying the set calibration curve in methanol and using the EE equation mentioned previously. The loading of all samples was done simultaneously under the same conditions and before FA conjugation. It was interestingly found that the percentages of EE for all samples were very close (44%). This value was consistent with a previous study in which LMS was loaded into FA conjugated polymer-coated (SPIONs).[19] However, several other studies have reported higher values when LMS was incorporated into different NPs without FA conjugation.[18,21,24]

Characterization of SNs

FTIR analysis

Based on the FA structure in Fig. 2, the infrared spectrum revealed some of its definite peaks as shown in Fig. 3. These peaks appeared at less than 2900 cm^{-1} and others at about (3200–3550 cm^{-1}), which related to NH and OH bonds.[25,26] Also, strong peaks were observed at 1650–1700 cm^{-1} due to carboxylic acid and carbonyl groups.[27] It was obvious that the FTIR spectra of conjugated NPs possessed the main peaks of FA with clear intensities compared with the FTIR pattern of the unconjugated ones.

All unconjugated samples have some of their functional groups, with the rest being silanol groups (Si−O−H).[28] Thus, bands at 3450 cm^{-1} and at 1650 cm^{-1} were observed due to both OH stretching

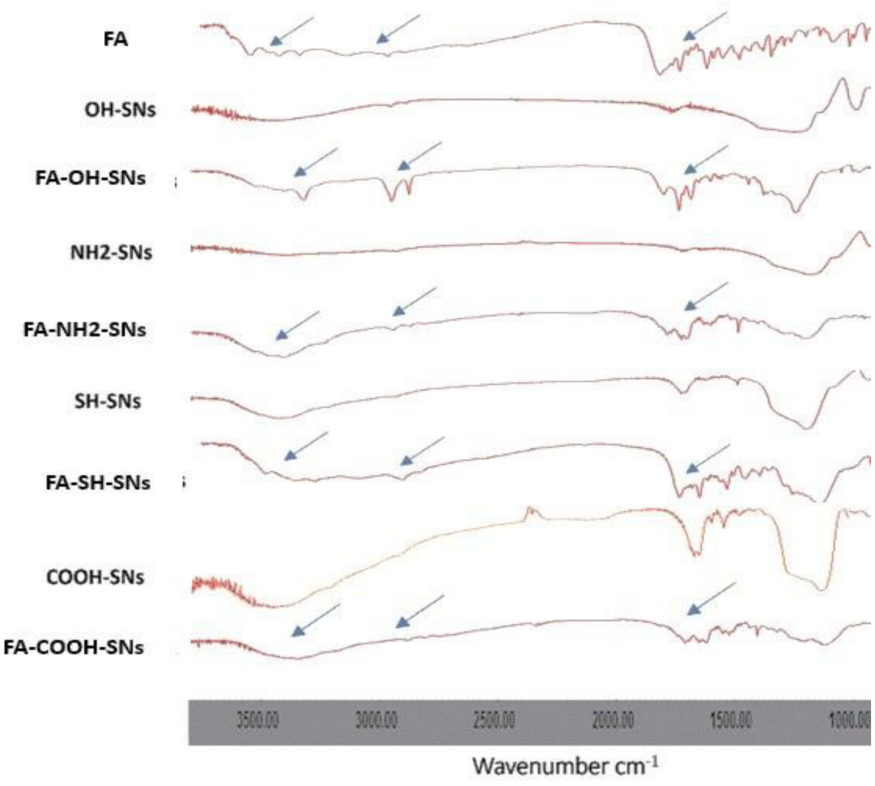

Fig. 3. FTIR spectra of FA, unconjugated, and conjugated SNs, where FA-conjugated NPs exhibited characteristic peaks corresponding to FA.

and bending, respectively. These peaks became more intense after FA conjugation due to their overlap. The strong bands at 1200 cm^{-1} and 1080 cm^{-1} were attributed to symmetric and asymmetric Si-O stretching motions.[29,30]

For NH_2-SNs and OH-SNs, the related peaks of FA appear clearly after its conjugation. However, A broad peak at 3100–3500 cm^{-1} and a band near 1650 cm^{-1} appeared in the FA–NH_2–SNs spectrum. These correspond to N–H and C=O stretches of the newly formed amide bond. They overlap with FA signals in the same regions, causing the increased broadness.

More peaks appeared for FA-OH-SNs at less than 2900 cm^{-1} and 1750 cm^{-1} due to C-H and C=O stretches, respectively, which were attributed most likely to the formed ester bond between FA and silanol groups. Also, some peaks appeared broader and more intense after FA conjugation to SH-NPs and COOH-SNs because of the ester formed with thiol and carboxyl groups, respectively. Notably, the strong peaks at 1650–1700 cm^{-1} for COOH-SNs corresponded to carboxylic acid groups. Thus, based on the reactions performed, as mentioned in the experimental part, and infrared spectra, a successful conjugation of FA with all samples has been achieved.

DLS analysis

DLS is a technique used to measure the hydrodynamic size of NPs in suspension by shining a laser through the sample and analyzing how the scattered light intensity changes over time.[31] It is also used to determine the PDI, which is a dimensionless number used to define the particle size distribution and its homogeneity in the mixture.[32] Its value may vary from 0.01 to 0.5–0.7, where a value > 0.7 indicates a broad particle size distribution of the formulation.[32]

Zeta-potential, which is the charge that arises between the surface of the NPs and their media, is another crucial parameter that can also be measured by DLS. It is used to characterize NPs' surface charge, obtain information about their stability, and surface interaction with other molecules. Zeta potential reflects the repulsion between charged particles, with higher values indicating greater stability and lower aggregation.[33,34] The surface charge of NPs is strongly influenced by the pH of the surrounding medium, which affects their zeta potential behavior.[35]

The mean particle size of these commercially available NPs (unloaded and unconjugated) was measured by DLS and observed to be nearly close to their

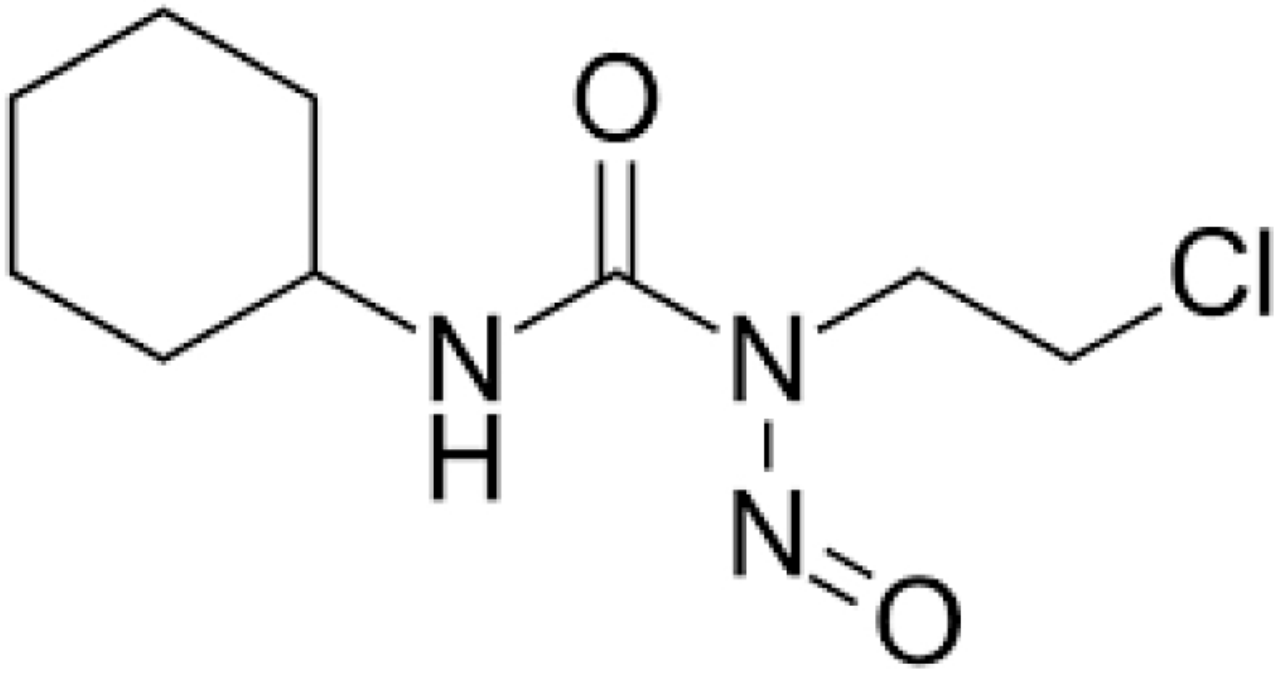

Fig. 4. LMS structure (https://www.ebi.ac.uk/chebi/searchId.do?chebiId=CHEBI:6520).

original size (200 nm), as shown in Table 1. The size increased slightly after LMS loading for all samples, indicating the possibility of adsorption of drug molecules on the NPs' surface. The adsorption might arise from the interaction between the different functional groups on the surface of SNs and the LMS groups *via*, most likely, the hydrogen bonds based on the LMS structure shown in Fig. 4. However, we believe that most drug molecules were encapsulated within the nanoparticle pores rather than adsorbed on the surface. This is supported by the characteristics of the NPs and the slight increase in particle size observed after loading.

The PDI of the original samples was generally below 0.4. It slightly increased after drug loading and FA conjugation yet remained within the desirable range of (0.2–0.5) (Table 1).

Regarding zeta potential values, all NPs gained originally negative values with a range from (–11 to –18) depending on the type of the functional group, as shown in Table 1.

As mentioned in the experimental part, the DLS was performed in PBS (pH 7.4), and thus the obtained values depended on the charges that existed at this pH, which was related to the type of functional group. OH-SNs have only silanol groups on their surfaces with a pKa value of 5.6. This resulted in a negative surface charge as these groups would be mainly deprotonated at neutral pH. On the other hand, the pKa of propyl thiol and propyl amine groups were 10.2

Table 1. DLS analysis of SNs in PBS (pH = 7.4) before and after LMS loading and FA conjugation, data were shown as mean ± SD (n = 3).

	Before drug loading			After drug loading			After folic acid conjugation		
SNs	Mean particle size (nm) ± SD	PDI ± SD	Zeta potential (mV) ± SD	Mean particle size (nm) ± SD	PDI ± SD	Zeta potential (mV) ± SD	Mean particle size (nm) ±SD	PDI ± SD	Zeta potential (mV) ± SD
COOH-SNs	206.47± 10.86	0.23± 0.12	–18.05± 0.60	254.13± 3.89	0.44± 0.08	–13.77± 0.98	309.3± 36.57	0.48± 0.01	–15.03± 0.80
SH-SNs	215.57± 3.47	0.2± 0.06	–13.63± 0.40	246.6± 10.84	0.45± 0.05	–8.83± 0.03	288.16± 18.86	0.45± 0.16	–12.76± 0.75
NH_2-SNs	202.13± 21.10	0.38± 0.10	– 11.03± 0.50	223.3± 6.98	0.48± 0.10	–4.39± 0.97	279.8± 12.86	0.39± 0.07	–14.1± 1.18
OH-SNs	203.40± 2.42	0.21± 0.04	–13.33± 1.06	228.4± 8.73	0.39± 0.08	–14.2± 0.66	284.83± 11.75	0.51± 0.08	–16.8± 0.36

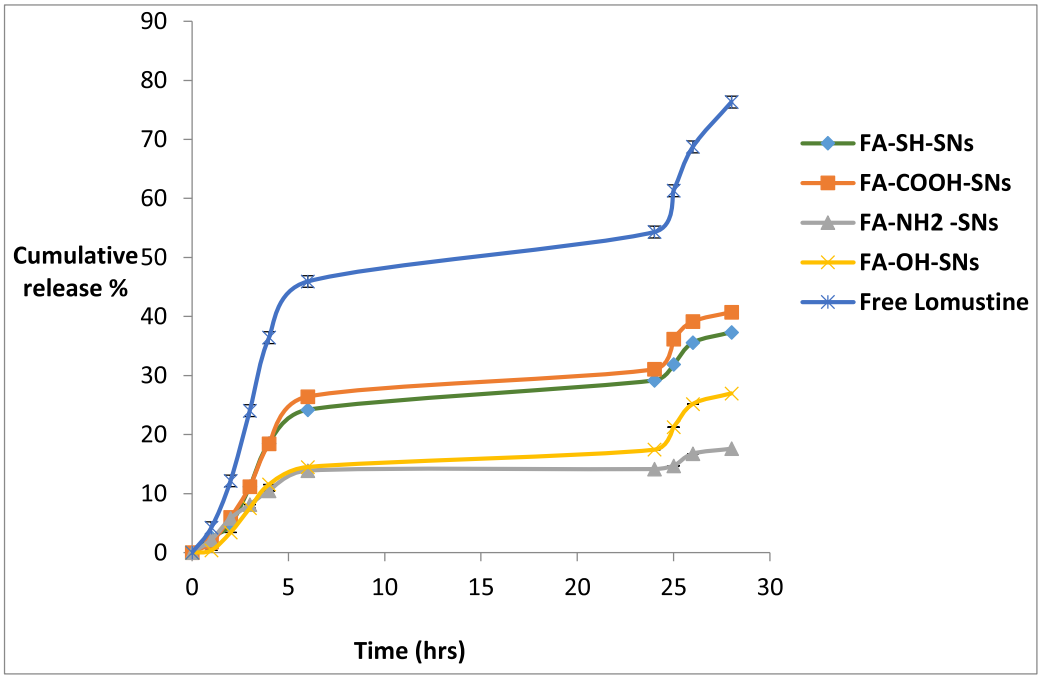

Fig. 5. The cumulative release of LMS from FA-conjugated SNs and as a free drug was measured, with data presented as mean ± SD (n = 3). Statistically significant differences were observed ($p < 0.05$) between the samples as obtained, using one-way ANOVA.

and 10.56, respectively. These groups were present in low amounts on the SN surface, the rest being silanol groups.[36] At neutral pH, both mainly carry a positive charge, so the net negative charge is not higher than that of OH-SNs. The highest negative value was for COOH-SNs, which was expected since the pKa of propyl carboxylic acid is 4.8[37] and thus will be deprotonated at neutral pH.

After LMS loading, the NPs became less negative. The pKa value of LMS is about 10.88, and it would be mainly protonated at neutral pH. Thus, if adsorbed on the surface of the NPs, it will diminish the magnitude of the negative charge, as shown in Table 1. The charge became more negative for all samples after FA conjugation. FA is an organic acid, and its dissociation constants (pKa) are 4.7, 6.8, and 8.7, and hence will primarily exist as an anion at neutral conditions.[38] The increase in negative charge after FA conjugation confirms successful modification of all samples, in agreement with the FTIR spectra. The variation in the net increase between samples highlights the effect of surface functional groups on the degree of FA conjugation.

NH_2-SNs showed the largest change in zeta potential after FA conjugation, changing from about −4 to −14 mV (over threefold). This suggests that they likely conjugate the highest amount of FA molecules. On the other hand, the magnitude of the zeta potential difference before and after FA conjugation with the other samples changed by less than 1.5 times.

In vitro drug release study

LMS release was studied at pH 7.4 using phosphate buffer saline (PBS) at 37 °C, as the release medium, to simulate the physiological conditions. The release patterns of LMS from FA conjugated SNs and as a free drug are represented in Fig. 5. They were measured as cumulative release percentages at different time intervals (1, 2, 3, 4, 6, 24, 25, 26, and 28 hours) based on a calibration curve in PBS. The findings demonstrated that the free drug dissolved faster than the drug-loaded SNs. Within the first 6 hours, more than 40% of the drug was released, then increased after 24 hours to come to about 76% after 28 hours. On the other hand, LMS-loaded SNs exhibited a slower release pattern at the same time intervals. The amount of released LMS from SNs within the first 6 hours was only in the range of (14%–26%) and reached the maximum at 28 hours to a range of (18%–41%). This result was consistent with a previous study using other types of NPs loaded with LMS.[19]

One- way ANOVA Calculator was used to assess the differences between all samples, and the values were found to be much less than 0.05 between all of them at all time intervals, indicating a statistically significant difference among them. Also, the differences were more significant when a free LMS was included and more significant after 6 hours compared to the first few hours.

FA-NH_2-SNs exhibited the slowest rate, while FA-COOH-SNs showed the fastest rate. As shown by zeta potential, NH_2-SNs had the greatest increase in negative charge after FA conjugation and correspondingly the slowest release rate. This suggests that a higher degree of FA conjugation can hinder drug release, leading to a slower release profile. NH_2-SNs have been conjugated with FA using the (EDC) coupling reaction, which was used to conjugate the two carboxylic acid groups of FA with the primary amine groups of NHS-SNs, leading to amide bond formation, which is a strong covalent bond.[39] In comparison, less stable FA conjugation on COOH-, OH-, and SH-SNs (via anhydride, ester, and thioester bonds) led to smaller zeta potential changes and faster drug release than NH_2-SNs.

Generally, the drug release rate from NPs depends on different factors, including the extent of drug solubility.[40] Since LMS is soluble in PBS at 37 °C,[41] a burst release behavior was observed within the first 6 hours and a release gain after 24 hours. The release data was fit to the Higuchi release model, which determined permeation as the process of drug release from an insoluble matrix by diffusion. As the release rate became slower after 24 hours, and it generally exhibited a slower rate for all samples compared to the free drug, this targeted system would be clinically useful in terms of prolonging the action of the drug. The extent of drug release slowdown depended on the type of functional group, as shown in Fig. 5. Furthermore, the targeting achieved here *via* FA ligands was beneficial by aiding the anticancer agents to reach basically the site of action and hence minimize their toxicities compared to the free form.

Comparable studies using nitrosourea drugs and structurally similar agents have been reported. For instance, FA-conjugated carmustine (BCNU) liposomes showed rapid initial release with limited control over sustained release.[42] Additionally, FA-functionalized hollow TiO_2 loaded with temozolomide exhibited controlled release profiles due to the core porosity and polymeric coatings.[43]

In vitro cell viability assay

Generally, *in vitro* cell toxicity depends on factors such as the type of cells and the characteristics of the drug carrier system.[44] Herein, suspensions of LMS-loaded, FA-conjugated SNs (0.15 mg/mL) and free drug were incubated with HeLa and VERO cells in separate culture flasks for 48 hours under identical conditions. MTT assay was then performed to assess the cell toxicity, and p-values were calculated between two different individual groups as well as between all groups.

HeLa cells were chosen in this study as they were cervical human cancerous cells that overexpress FRs on their surfaces. On the other hand, VERO cells were isolated from normal kidney epithelial cells of an African green monkey, and they were not immortal cells like HeLa.[45] Also, they are one of the most used mammalian continuous cell lines in cytotoxicity studies.[46]

When incubating HeLa cells and performing a comparison between the conjugated SNs, the value was ≤ 0.05 only between FA-NH_2-SNs and FA-SH-SNs, and between FA-NH_2-SNs and FA-COOH-SNs. When comparing the conjugated NPs with the free drug, the value was less than 0.05 only between FA-NH_2-SNs and the free drug, while the p-value between all conjugated samples and the free drug, when all compared at once, was ≤ 0.05.

On the contrary, the differences were more significant when conducting the assay on VERO cells, where the value was less than 0.05 between all individual conjugated NPs and between each of them and the free drug, except between FA-COOH-NPs and FA-SH-NPs, FA-COOH-NPs and FA-OH-NPs, and FA-SH-NPs and FA-OH-NPs.

As shown in Fig. 6, the highest cell toxicity percentage against HeLa cells was associated with free LMS (about 70%). Interestingly, for conjugated SNs, the order of cell toxicity effect was almost related to their release rate behaviors, where the order was as follows: FA-NH_2-SNs $<$ FA-OH-SNs $<$ FA-SH-SNs $\sim$ FA-COOH-SNs with a range of about (40–58%).

As mentioned previously, NH_2-SNs formed the most stable covalent bonds with FA, resulting in slower drug release, as confirmed by the largest change in negative charge after conjugation. Interestingly, the same order was observed in normal (VERO) cells, but with much lower cytotoxicity, reaching less than half of the level measured in cancer cells. In cancer therapy, targeting is crucial so that normal cells are protected, and most of the therapeutic doses reach their site of action via specific ligands like FA, which has its folate receptors on the surface of different cancerous cells like HeLa cells.[47]

Thus, the extent of FA conjugation, determined by the surface functional group of SNs, clearly influenced both the drug release rate and its cytotoxicity. The overall low cytotoxicity of FA-conjugated SNs might not be due only to their slow cumulative release behavior but also to the effect of their surface charge. Generally, positively charged NPs have more capability to internalize into the cells compared to negatively charged NPs.[48,49] At neutral pH, LMS will be mainly protonated and gain a positive charge, while FA will be deprotonated with a net negative charge, and hence will show a lower

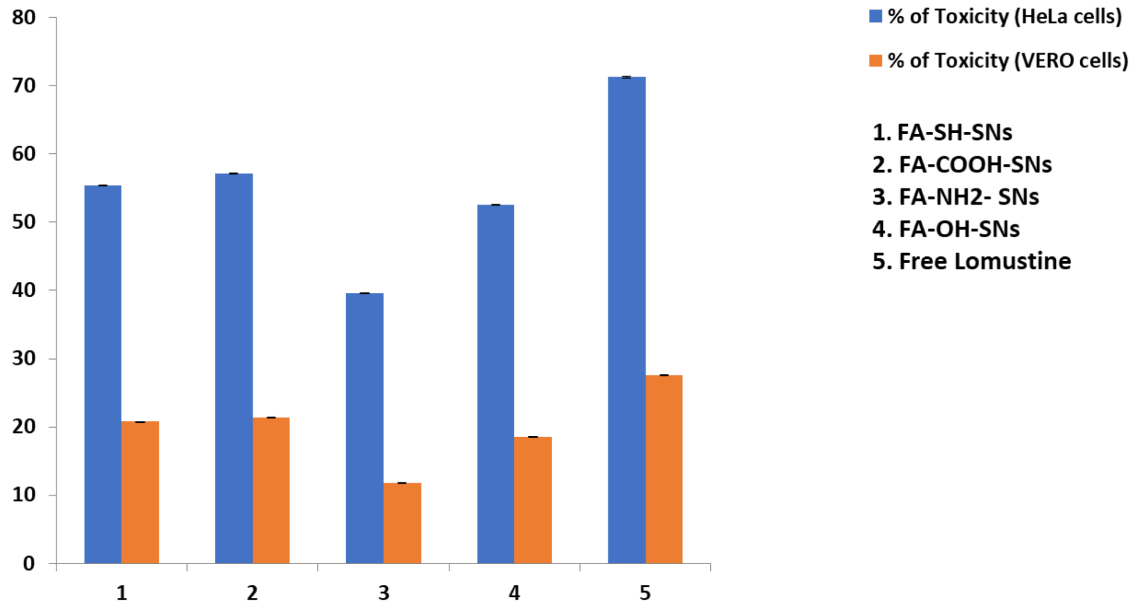

Fig. 6. The MTT cell viability assay was performed on HeLa and VERO cells after incubation for 48 hours with 0.15 mg/mL of FA-conjugated SNs and free LMS. Data are presented as mean ± SD (n = 3), and statistical significance was measured using one-way ANOVA.

cellular internalization.[50] Similar systems have been reported for other FA-functionalized carriers, such as lomustine-loaded SPIONs and temozolomide-loaded FA-TiO_2 [19,43] where folate-mediated uptake improved cell targeting, but release kinetics influenced overall cytotoxic effect. Thus, surface functionalization allows balancing targeted uptake with controlled cytotoxicity, providing a tunable strategy for nitrosourea or similar chemotherapeutics.

Even though free LMS exhibited a higher toxicity and release rate compared to the conjugated SNs, their slower release rate would prolong the action of the drug and reduce its side effects and the frequency of the doses. Furthermore, the favorable properties of SNs can be utilized to enhance drug delivery, including their high encapsulation efficiency and ability to be conjugated with different ligands for targeted delivery. In addition, SNs act as protective carriers that prevent drug degradation and rapid clearance, which ultimately reduces the required dose. Therefore, the targeting achieved from FA ligands toward cancerous cells can be further optimized/controlled in terms of drug release rate and cell toxicity by choosing the functional group, which can be a simple linker group, as was done here.

Conclusion

In our present study, we explored how the surface functional groups on SNs influence their ability to bind FA and how this, in turn, affects the *in vitro* characteristics of LMS. Four types of commercially modified SNs were tested (NH_2-, SH-, COOH-, and OH-SNs). All of them were able to encapsulate LMS with an efficiency of about 44%, and a successful FA conjugation was confirmed by FTIR.

DLS measurements showed an increase in the mean particle size after loading the drug and FA conjugation. While LMS loading resulted in a less negative surface charge, FA conjugation caused a more negative charge, with NH_2-SNs showing the largest change, most likely due to a higher level of FA conjugation through amide bond formation.

Both drug release and cytotoxicity differed depending on the functional group, following the order: FA–NH_2-SNs < FA–OH-SNs < FA–SH-SNs ≈ FA–COOH-SNs. A stronger ability to conjugate FA generally resulted in a slower drug release and a lower cytotoxicity. All FA-conjugated samples released the drug more slowly and were less cytotoxic than free LMS. As expected for FA-targeted systems, the formulations were more toxic against HeLa cancerous cells compared to normal VERO cells.

Overall, the results demonstrated that the type of surface functional group plays a key role in determining the extent of FA conjugation and, consequently, the release behavior and cytotoxicity of LMS-loaded SNs.

Acknowledgment

The authors gratefully acknowledge Applied Science Private University, Amman, Jordan, for funding this project (Grant

No. DRGS-2015-2016-35). We also thank the Pharmacological and Diagnostic Research Center (PDRC) at Al-Ahliyya Amman University, Amman, Jordan, for performing confirmatory analysis, and Prof. Wamidh Talib (Applied Science Private University, Amman, Jordan) for his assistance with the MTT assay, which was carried out by the authors in his laboratory.

Authors' declaration

- Conflicts of Interest: None.
- We hereby confirm that all the Figures and Tables in the manuscript are ours. Furthermore, any Figures and images that are not ours have been included with the necessary permission for republication, which is attached to the manuscript.
- No animal studies are present in the manuscript.
- No human studies are present in the manuscript.
- Ethical Clearance: The project was approved by the local ethical committee at Al-Ahliyya Amman University, Amman, Jordan.

Authors' contributions statement

A. Kh. conceived and designed the experiments and wrote the manuscript. L. I. conducted the experiments. E. M. reviewed, edited, and proofread the manuscript.

References

1. Altammar KA. A review on nanoparticles: characteristics, synthesis, applications, and challenges. Front Microbiol. 2023 Apr;14:1155622. https://doi.org/10.3389/fmicb.2023.1155622.
2. Alshaer W, Alsotari S, Aladaileh N, Rifai A, Khalaf A, AlQuaissi B, *et al.* Clarithromycin-loaded albumin-based nanoparticles for improved antibacterial and anticancer performance. Pharmaceutics. 2025 May;17(6):729. https://doi.org/10.3390/pharmaceutics17060729.
3. Oleiwi MA, Al-Samydai AM, Al-Kabariti AY, Al Azzam KM, Carradori S, Alshaer W. Codelivery of raloxifene and rutin as PEGylated nanoliposomes: formulation, characterization, and prophylactic activity against breast cancer. Adv Pharm Bull. 2025 Jun;15(2):371–389. https://doi.org/10.34172/apb.025.43681.
4. Tadesse S, Hailemariam T. A review on the classification, characterisation, synthesis of nanoparticles and their application. Advances. 2025 Jun;6(2):63–72. https://doi.org/10.11648/j.advances.20250602.15.
5. Ibraheem LM, Khattabi AM. Studying the effect of functional group and size of silica nanoparticles loaded with quercetin on their in vitro characteristics. Jordan J Pharm Sci. 2022 Dec;15(4):569–582. https://doi.org/10.35516/jjps.v15i4.679.
6. Joudeh N, Linke D. Nanoparticle classification, physicochemical properties, characterization, and applications: a comprehensive review for biologists. J Nanobiotechnology. 2022 Jun;20(1):262. https://doi.org/10.1186/s12951-022-01477-8.
7. Porrang S, Davaran S, Rahemi N, Allahyari S, Mostafavi E. How advancing are mesoporous silica nanoparticles? A comprehensive review of the literature. Int J Nanomedicine. 2022 Apr;17:1803–1827. https://doi.org/10.2147/IJN.S353349.
8. Ahmed AJ, Alias MF. Synthesis, structural, morphological characterization, and cytotoxicity assays of metal complexes decorated SiO2 nanoparticles against breast cancer cell lines (MDA-MB-231). Baghdad Sci J. 2024 Aug;21(8):2568. https://doi.org/10.21123/bsj.2024.8834.
9. Gupta J, Quadros M, Momin M. Mesoporous silica nanoparticles: synthesis and multifaceted functionalization for controlled drug delivery. J Drug Deliv Sci Technol. 2023 Mar;81:104305. https://doi.org/10.1016/j.jddst.2023.104305.
10. Florensa M, Llenas M, Medina-Gutiérrez E, Sandoval S, Tobías-Rossell G. Key parameters for the rational design, synthesis, and functionalization of biocompatible mesoporous silica nanoparticles. Pharmaceutics. 2022 Dec;14(12):2703. https://doi.org/10.3390/pharmaceutics14122703.
11. Yuan M, Han Z, Liang Y, Sun Y, He B, Chen W, *et al.* mRNA nanodelivery systems: targeting strategies and administration routes. Biomater Res. 2023 Feb;27(1). https://doi.org/10.1186/s40824-023-00425-3.
12. Yan S, Na J, Liu X, Wu P. Different targeting ligands-mediated drug delivery systems for tumor therapy. Pharmaceutics. 2024 Feb;16(2):248. https://doi.org/10.3390/pharmaceutics16020248.
13. Zhang Z. Progress of folic acid-folate receptor as drug carriers in targeted drug delivery system. In SHS Web Conf. 2022 Aug;144:01002. https://doi.org/10.1051/shsconf/202214401002.
14. Young O, Ngo N, Lin L, Stanbery L, Creeden JF, Hamouda D, *et al.* Folate receptor as a biomarker and therapeutic target in solid tumors. Curr Probl Cancer. 2023 Feb;47(1):100917. https://doi.org/10.1016/j.currproblcancer.2022.100917.
15. Liu Y, Chen X, Evan T, Esapa B, Chenoweth A, Cheung A, *et al.* Folate receptor alpha for cancer therapy: an antibody and antibody-drug conjugate target coming of age. MAbs. 2025 Dec;17(1). https://doi.org/10.1080/19420862.2025.2470309.
16. Hawner M, Ducho C. Cellular targeting of oligonucleotides by conjugation with small molecules. Molecules. 2020 Dec;25(24):5963. https://doi.org/10.3390/molecules25245963.
17. Ibrahim MAI, Othman R, Chee CF, Ahmad Fisol F. Evaluation of folate-functionalized nanoparticle drug delivery systems—effectiveness and concerns. Biomedicines. 2023 Jul;11(7):2080. https://doi.org/10.3390/biomedicines11072080.
18. Anand A, Iyer BR, Ponnusamy C, Pandiyan R, Sugumaran A. Design and development of lomustine loaded chitosan nanoparticles for efficient brain targeting. Cardiovasc Hematol Agents Med Chem. 2020 Aug;18(1):45–54. https://doi.org/10.2174/1871525718666200203112502.
19. Jafari S, Tavakoli MB, Zarrabi A. Lomustine loaded superparamagnetic iron oxide nanoparticles conjugated with folic acid for treatment of glioblastoma multiforma (GBM). Iran J Pharm Res. 2020;19(2):134–144. https://doi.org/10.22037/IJPR.2020.1101032.

20. Katona G, Sabir F, Sipos B, Naveed M, Schelz Z, Zupkó I, *et al.* Development of lomustine and n-propyl gallate co-encapsulated liposomes for targeting glioblastoma multiforme via intranasal administration. Pharmaceutics. 2022;14(3):631. https://doi.org/10.3390/pharmaceutics14030631.
21. Alaayedi MH, Maraie NK. Lomustine's nanoemulsion as nose-to-brain drug delivery system for CNS tumor treatment. Saudi Pharm J. 2023;31(8):101692. https://doi.org/10.1016/j.jsps.2023.06.025.
22. Parvathaneni V, Shukla SK, Gupta V. Development and characterization of folic acid-conjugated amodiaquine-loaded nanoparticles–efficacy in cancer treatment. Pharmaceutics. 2023;15(3):1001. https://doi.org/10.3390/pharmaceutics15031001.
23. Mehrotra A, Nagarwal RC, Pandit JK. Lomustine loaded chitosan nanoparticles: characterization and in-vitro cytotoxicity on human lung cancer cell line L132. Chem Pharm Bull (Tokyo). 2011;59(3):315–320. https://doi.org/10.1248/cpb.59.315.
24. Mehrotra A, Pandit JK. Preparation and characterization and biodistribution studies of lomustine loaded PLGA nanoparticles by interfacial deposition method. J Nanomedine Biotherapeutic Discov. 2015;5(4):1000138. https://doi.org/10.4172/2155-983X.1000138.
25. Ortiz-Islas E, Sosa-Arróniz A, Manríquez-Ramírez ME, Rodríguez-Pérez CE, Tzompantzi F, Padilla JM. Mesoporous silica nanoparticles functionalized with folic acid for targeted release Cis-Pt to glioblastoma cells. Adv Mater Sci. 2021;60(1):25–37. https://doi.org/10.1515/rams-2021-0009.
26. Abbasi M, Sohail M, Minhas MU, Iqbal J, Mahmood A, Shaikh AJ. Folic acid-functionalized nanoparticles-laden biomaterials for the improved oral delivery of hydrophobic drug in colorectal cancer. J Drug Deliv Sci Technol. 2022 May;71:103287. https://doi.org/10.1016/j.jddst.2022.103287.
27. Al Khatib AO, Yousfan A, Abed A, El-Tanani M, Al-Obaidi H. Development of pimozide spray dried lipid nanoparticles with enhanced targeting of non-small cell lung cancer. J Drug Deliv Sci Technol. 2025;109. https://doi.org/10.1016/j.jddst.2025.106969.
28. Mariadoss AVA, Saravanakumar K, Sathiyaseelan A, Venkatachalam K, Wang MH. Folic acid functionalized starch encapsulated green synthesized copper oxide nanoparticles for targeted drug delivery in breast cancer therapy. Int J Biol Macromol. 2020 Dec;164:2073–2084. https://doi.org/10.1016/j.ijbiomac.2020.08.036.
29. Trukawka M, Cendrowski K, Konicki W, Mijowska E. Folic acid/methotrexate functionalized mesoporous silica nanoflakes from different supports: comparative study. Appl Sci. 2020 Sep;10(18):6465. https://doi.org/10.3390/app10186465.
30. Khosravian P, Shafiee Ardestani M, Khoobi M, Ostad SN, Dorkoosh FA, Javar HA, *et al.* Mesoporous silica nanoparticles functionalized with folic acid/methionine for active targeted delivery of docetaxel. Onco Targets Ther. 2016 Dec;9:7315–7330. https://doi.org/10.2147/OTT.S113815.
31. Knysh A, Sokolov P, Nabiev I. Dynamic light scattering analysis in biomedical research and applications of nanoparticles and polymers. J Biomed Photonics Eng. 2023 May;9(2):020203. https://doi.org/10.18287/JBPE23.09.020203.
32. Karabatak N, Gök B, Budama-Kılınc Y. Development of nanoemulsion formulation containing ylang ylang essential oil for topical applications, evaluation of in vitro cytotoxicity and ADMET profile. J Turk Chem Soc A Chem. 2024 Aug;11(3):1181–1196. https://doi.org/10.18596/jotcsa.1418645.
33. Németh Z, Csóka I, Semnani Jazani R, Sipos B, Haspel H, Kozma G, *et al.* Quality by design-driven zeta potential optimisation study of liposomes with charge imparting membrane additives. Pharmaceutics. 2022 Aug;14(9):1798. https://doi.org/10.3390/pharmaceutics14091798.
34. Xiong Y, Liu X, Xiong H. Aggregation modeling of the influence of pH on the aggregation of variably charged nanoparticles. Sci Rep. 2021 Aug;11(1):17386. https://doi.org/10.1038/s41598-021-96798-3.
35. McLean B, Yarovsky I. Structure, properties, and applications of silica nanoparticles: recent theoretical modeling advances, challenges, and future directions. Small. 2024 Dec;20(51). https://doi.org/10.1002/smll.202405299.
36. Khattabi AM, Talib WH, Alqdeimat DA. A targeted drug delivery system of anti-cancer agents based on folic acid-cyclodextrin-long polymer functionalized silica nanoparticles. J Drug Deliv Sci Technol. 2017 Oct;41:367–374. https://doi.org/10.1016/j.jddst.2017.07.025.
37. Srivastava P, Tavernaro I, Scholtz L, Genger C, Welker P, Schreiber F, *et al.* Dual color pH probes made from silica and polystyrene nanoparticles and their performance in cell studies. Sci Rep. 2023 Jan;13(1):1321. https://doi.org/10.1038/s41598-023-28203-0.
38. Martins-Júnior HA, Wang AY, Alabourda J, Pires MAF, Vega OB, Lebre DT. A validated method to quantify folic acid in wheat flour samples using liquid chromatography: tandem mass spectrometry. J Braz Chem Soc. 2008;19(5):971–977. https://doi.org/10.1590/S0103-50532008000500024.
39. Ahmadi M, Ritter CA, von Woedtke T, Bekeschus S, Wende K. Package delivered: folate receptor-mediated transporters in cancer therapy and diagnosis. Chem Sci. 2024;15:1966–2006. https://doi.org/10.1039/d3sc05539f.
40. Maan O, Al-Samydai A, Alqaraleh M, Nsairat H, Alsanabrah A, Awwad O, *et al.* Co-loaded nanoparticles of empagliflozin and rutin for pancreatitis prevention and anticancer activity. Drug Dev Res. 2025;86(6). https://doi.org/10.1002/ddr.70155.
41. Mehrotra A, Nagarwal RC, Pandit JK. Fabrication of lomustine loaded chitosan nanoparticles by spray drying and in vitro cytostatic activity on human lung cancer cell line L132. J Nanomed Nanotechnol. 2010;1(1). https://doi.org/10.4172/2157-7439.1000103.
42. Honmane SM, Charde MS, Choudhari PB, Jadhav NR. Development and in vitro evaluation of folate conjugated polydopamine modified carmustine-loaded liposomes for improved anticancer activity. J Drug Deliv Sci Technol. 2023 Dec;90:105145. https://doi.org/10.1016/j.jddst.2023.105145.
43. Uribe-Robles M, Ortiz-Islas E, Rodriguez-Perez E, Valverde FF, Lim T, Martinez-Morales AA. Targeted delivery of temozolomide by nanocarriers based on folic acid-hollow TiO2 nanospheres for the treatment of glioblastoma. Biomater Adv. 2023 Aug;151:213442. https://doi.org/10.1016/j.bioadv.2023.213442.
44. Płuciennik K, Sicińska P, Misztal W, Bukowska B. Important factors affecting induction of cell death, oxidative stress and DNA damage by nano- and microplastic particles in vitro. Cells. 2024 Apr;13(9):768. https://doi.org/10.3390/cells13090768.
45. Osada N, Kohara A, Yamaji T, Hirayama N, Kasai F, Sekizuka T, *et al.* The genome landscape of the African green monkey kidney-derived Vero cell line. DNA Res. 2014 Dec;21(6):673–683. https://doi.org/10.1093/dnares/dsu029.

46. Gomes LM, Moysés DA, Nascimento HFS, Mota TC, Bonfim LT, Cardoso PCS, *et al.* Genotoxic and cytotoxic effects of the drug dipyrone sodium in African green monkey kidney (Vero) cell line exposed in vitro. Naunyn Schmiedebergs Arch Pharmacol. 2021 Jul;394(7):1529–1535. https://doi.org/10.1007/s00210-021-02078-2.
47. Jin X, Zhang J, Jin X, Liu L, Tian X. Folate receptor targeting and cathepsin B-sensitive drug delivery system for selective cancer cell death and imaging. ACS Med Chem Lett. 2020 Aug;11(8):1514–1520. https://doi.org/10.1021/acsmedchemlett.0c00031.
48. Hühn D, Kantner K, Geidel C, Brandholt S, De Cock I, Soenen SJH, *et al.* Polymer-coated nanoparticles interacting with proteins and cells: focusing on the sign of the net charge. ACS Nano. 2013 Apr;7(4):3253–3263. https://doi.org/10.1021/nn3059295.
49. Moscatiello GY, Natale C, Inserra M, Morelli A, Russo L, Battajini N, *et al.* The surface charge both influences the penetration and safety of polystyrene nanoparticles despite the protein corona formation. Environ Sci Nano. 2025;12(5):2857–2870. https://doi.org/10.1039/D4EN00962B.
50. Truszkowska M, Saleh A, Ebert ML, Kali G, Bernkop-Schnürch A. Addressing the polycation dilemma in drug delivery: charge-converting liposomes. J Mater Chem B. 2025;13(30):9100–9111. https://doi.org/10.1039/D5TB00945F.

دراسة تأثير المجموعة الوظيفية على ارتباط حمض الفوليك وعلى الخصائص المخبرية للوماستين من جسيمات السيليكا النانوية

عرين خطابي[1]، لينا ابراهيم[2] ، إيمان مقدادي[2]

[1]مركز البحوث الدوائية والتشخيصية ، كلية الصيدلة ، جامعة عمان الأهلية، عمان، الأردن، 19111
[2] قسم العلوم الصيدلانية والصيدلانيات، كلية الصيدلة، جامعة العلوم التطبيقية الخاصة، عمان، الأردن، الرمز البريدي: 11937

الخلاصة

في هذه الدراسة، جرى تحميل جسيمات السيليكا النانوية (SNs) ذات المجموعات الوظيفية المختلفة (بروبيل أمين، بروبيل ثيول، بروبيل حمض كربوكسيلي، ومجموعة الهيدروكسيل) بمضاد السرطان لوموستين (LMS) ثم ربطها بحمض الفوليك (FA) لإنتاج كلٍّ من FA-NH_2-SNs و FA-SH-SNs وFA-COOH-SNs وFA-OH-SNs على التوالي. وقد جرى توصيف الجسيمات النانوية باستخدام الأشعة تحت الحمراء (FTIR) و جهاز التشتت الضوئي الديناميكي (DLS) ، و تم تحديد كفاءة التغليف (EE) ومعدل الاطلاق باستخدام المطياف فوق البنفسجي. كما تم تقييم السميّة الخلوية في المختبر تجاه خلايا HeLaو VERO باستخدام اختبار MTT وقد تجاوزت كفاءة تغليف الـ LMS نسبة 40%، وأكدت أطياف FTIR نجاح ارتباط حمض الفوليك. ازداد حجم الجزيئات بعد تحميل الـ LMS وربط حمض الفوليك، حيث تراوح بين 284 و308 نانومتر. وأظهرت قياسات الجهد السطحي (Zeta potential) أن جميع الجسيمات النانوية أصبحت أكثر سالبية بعد ربط حمض الفوليك، وكان أكبر تغير في جسيمات NH_2-SNs (من نحو −4 إلى −14 ميليفولت). كما أظهر تحليل التباين الأحادي (One-way ANOVA) فروقًا إحصائية ($p < 0.05$) بين معظم التراكيب في كلٍّ من معدلات اطلاق الدواء والسميّة الخلوية، والتي كانت أقل مقارنة بالدواء الحر. وكانت السميّة الخلوية أعلى ضد خلايا HeLa مقارنة بخلايا VERO، نتيجة الاستهداف المعتمد على مستقبلات الفولات. كان ترتيب التأثيرات السمية الخلوية مرتبطًا بسلوك معدلات الإطلاق الدوائي ، حيث سجّلت جسيمات FA-NH_2-SNs أقل القيم (18% و40% على التوالي). وبذلك تَبيَّن أن نوع المجموعة الوظيفية السطحية يؤثر بدرجة كبيرة في كفاءة ارتباط حمض الفوليك، مما يؤدي بدوره إلى تعديل الخصائص المخبرية للدواء المحمّل، حيث ارتبطت زيادة ارتباط حمض الفوليك بانخفاض معدلات الاطلاق والسميّة الخلوية.

الكلمات المفتاحية: الإطلاق التراكمي، السمية الخلوية، التحليل بجهاز التشتت الضوئي الديناميكي (DLS)، الأشعة تحت الحمراء FTIR ، اللوماستين ، جسيمات السيليكا النانوية، المجموعات الوظيفية على السطح.